

# EVOLUTION OF HARD X-RAY SPECTRA ALONG THE BRANCHES IN CIR X-1

G. Q. Ding <sup>1,2</sup>, J. L. Qu <sup>1</sup>, and T. P. Li <sup>1,3</sup>

*dingqq@mail.ihep.ac.cn, qujl@mail.ihep.ac.cn, litp@mail.ihep.ac.cn*

## ABSTRACT

Using the data from the PCA and HEXTE on board the RXTE satellite, we investigate the evolution of the 3-200 keV spectra of the peculiar low mass X-ray binary (LMXB) Cir X-1 along the branches on its hardness-intensity diagram (HID) from the vertical horizontal branch (VHB), through the horizontal horizontal branch (HHB) and normal branch (NB), to the flaring branch (FB). We detect a power-law hard component in the spectra. It is found that the derived photon indices ( $\Gamma$ ) of the power-law hard component are correlated with the position on the HID. The power-law component dominates the X-ray emission of Cir X-1 in the energy band higher than  $\sim 20$  keV. The fluxes of the power-law component are compared with those of the bremsstrahlung component in the spectra. A possible origin of the power-law hard component is discussed.

*Subject headings:* binaries: general — stars: individual (Circinus X-1) — X-rays: binaries — X-rays: general — X-rays: individual (Circinus X-1)

## 1. INTRODUCTION

Circinus X-1 (Cir X-1), with an orbital period of 16.6 days and a distance of 5.5 kpc (Case et al. 1998), is thought to be a peculiar X-ray binary. Because its rapid variability is similar to that of Cyg X-1, its compact object was considered to be a black hole (Toor 1977). However, the compact object is also believed to be a neutron star because of the presence of type I X-ray bursts (Tennant et al. 1986 a, 1986 b). The radio counterpart of Cir X-1,

---

<sup>1</sup>Laboratory for Particle Astrophysics, Institute of High Energy Physics, Chinese Academy of Sciences, Beijing, China

<sup>2</sup>Graduate School of Chinese Academy of Sciences, Beijing, China

<sup>3</sup>Department of Physics & Center for Astrophysics, Tsinghua University, Beijing, China

coincident with a faint red star, displays flares with the same periodicity as the orbital period (Whelan et al. 1977); its IR characteristics also showed periodicity (Glass 1978); and its optical counterpart is proven to be a faint red star (Moneti 1992). The soft X-ray (3-6 keV) flux of Cir X-1 shows a well-defined periodic modulation with the same period as its orbital period (Kaluziński et al. 1976). The large X-ray to optics luminosity ratio suggests that Cir X-1 is a LMXB.

According to their fast timing properties and shapes of X-ray color-color diagram (CCD) or the hardness-intensity diagram (HID), LMXBs whose primary compact objects are neutron stars can be divided into two classes: Z source and atoll source (Hasinger & van der Klis 1989). There have been different opinions about what kind of LMXB Cir X-1 belongs to. From its temporal behaviors along its HID, Shirey(1998) believed that Cir X-1 is a Z source; but Oosterbroek et al.(1995), after having studied its X-ray spectra and fast timing variations with EXOSAT ME data, suggested that Cir X-1 is the only known atoll source with a very low magnetic field strength of less than  $10^9$  G.

The accretion geometry of LMXBs can be inferred from studies of their hard X-ray spectra. Detailed studies of hard X-ray spectra of both Z and atoll sources have been reported (Barret et al. 2000; Di Salvo et al. 2000; D’Amico et al. 2001; Di Salvo et al. 2001). Using data of different high energy X-ray satellites (Barret et al. 1999), the X-ray and hard X-ray spectra of LMXBs, including six Z sources (Sco X-1, GX 349+2, GX 340+0, Cyg X-2, GX 5-1, and GX 17+2), have been analyzed on the different branches of HID or CCD.

Using the RXTE data, Shirey et al.(1999) investigated the continuous evolutions of the Fourier power spectra and energy spectra of X-ray (2.5-25 keV) along the branches of the HID of Cir X-1, which displays a complete “Z” track. The quasi-periodic oscillation (QPO) frequencies from 12 Hz to 30 Hz have been detected on the HB, 4 Hz on the NB, and no QPO on the FB. Also using RXTE observation data, Qu et al.(2001) studied the evolution of time lags along the complete HID; the time lag observed in Cir X-1 seems to be consistent with the Comptonization model with a two-layer corona.

With the ASCA observations for Cir X-1, Brandt et al.(1996) investigated the spectral behavior for partial covering near zero phase of Cir X-1, Iaria et al.(2001 a) reported the spectral evolution along its orbit. Using the BeppoSAX data, Iaria et al.(2001 b, 2002) analyzed the spectra of Cir X-1 at the periastron and broadband spectrum at orbital phases close to the apoastron. However, the high energy spectra of Cir X-1 have been poorly understood. In this work, using the PCA and HEXTE observations on board the RXTE, we investigate the evolution of broadband spectrum (3-200 keV) of Cir X-1 along its HID from the VHB, through the HHB and NB, to the FB. The data selection and analysis are

described in §2, and results and discussion presented in §3.

## 2. OBSERVATIONS AND DATA ANALYSIS

We choose the Standard Mode 2 data of the PCA and Standard Modes (Archive) data of the HEXTE to perform our analysis. Because detector 2 of cluster B of the HEXTE loses its spectral capability and automatic gain control, only cluster A data are analyzed. The used observations are listed in Table 1. The ftools Version5.2 is used to perform our data analysis. The observations for which RXTE pointing offsets are larger than  $0.02^\circ$  and elevation angles less than  $10^\circ$  are discarded.

Using the method described by Shirey et al.(1999) with soft color being defined as the ratio of the counts in the (6.5-13.0)/(2.0-6.5) keV energy bands, we use the PCA data to obtain the HID of Cir X-1, in which the soft color is plotted against the intensity in the 2-18.6 keV energy interval. Figure 1 shows the obtained HID with four branches sequentially called VHB, HHB, NB, and FB from the top left to the bottom right of the diagram. In the VHB, the source intensities show little variation with the soft color; in the HHB, the soft color remains almost constant with the source intensity. The soft color is positively correlated with the source intensity in the NB. The FB is connected to the soft end of the NB, where erratic variations are seen in both the hardness ratio and the source intensity.

We derive the hard X-ray spectrum of a certain branch according to the positions in the HID for each observation. The resultant hard X-ray spectrum of a branch is then obtained by adding all the spectra of the same branch from different OBSIDs. In order to enhance the signal-to-noise ratio (SNR) of the HEXTE spectra, the energy channels higher than 15 keV in the HEXTE spectra are rebinned. The energy channels are rebinned in accordance with the principle: the higher the energy channels, the more the rebinned energy channels.

The spectra of 3-20 keV are derived from the PCA data (PCU0 only) and those of 20-200 keV from the HEXTE data. The dips are discarded when the the X-ray spectra are extracted. The HEXTE gaps and bad HEXTE observation intervals which are with zero photon count rate are discarded when HEXTE spectra are extracted. We use Xspec 11.2 to analyze the four broadband (3-200 keV) spectra. A systematic error of 1% is added to each PCA spectrum due to the calibration uncertainties. The PCA X-ray spectrum and HEXTE hard X-ray spectrum of every branch are simultaneously fit by a combination model of a blackbody plus a line, a bremsstrahlung, a power-law, and an absorption edge. The fit results are shown in Figures 2 - 5 and Table 2. From the obtained spectra, we can estimate the absorbed fluxes of the bremsstrahlung component of 3-200 keV, the power-law component

of 20-200 keV, and the luminosity of 3-200 keV. The results are listed in Table 3. The F-test (Protassov et al. 2000) provided by Xspec 11.2 is performed to test the rationality of adding an extra power-law component in the spectral fitting. For each branch, the fitting  $\chi^2$  and d.o.f of the Bblody+Line+Bremss+Edge model with and without an extra Power-law component, and the corresponding F-test probability are listed in Table 4.

### 3. RESULTS AND DISCUSSION

From the F-test probability listed in Table 4, it is shown that adding an extra power-law hard component is reasonable in the spectral fitting for each branch, which means that the hard X-ray tail of Cir X-1 is detected and its presence is not associated with a particular position on its HID. The derived photon indices ( $\Gamma$ ) of the four branches span a range from 0.95 to 2.11 (see Table 2). The hardest index of the four branches is obtained when the source is on the NB, and the softest is on the VHB.

The mass accretion rate  $\dot{M}$  increases in the sequence VHB  $\rightarrow$  HHB  $\rightarrow$  NB  $\rightarrow$  FB (van der Klis et al. 1996); the power law index continuously decreases in the sequence VHB  $\rightarrow$  HHB  $\rightarrow$  NB (see Table 2). In other words, the hard X-ray spectrum hardens from VHB, through HHB, to NB with the increase of the mass accretion rate  $\dot{M}$ . So, there may exist a correlation between the hardness of the hard X-ray spectrum and the mass accretion rate  $\dot{M}$ . Our results show that the hard X-ray evolution of Cir X-1 from the horizontal branch (HB) to the NB is similar to that of Sco X-1 from the HB to the NB (D’Amico et al. 2001).

From table 3, it is shown that hard X-ray luminosity fluxes fade in the sequence VHB  $\rightarrow$  HHB  $\rightarrow$  NB; in other words, the less the mass accretion rate  $\dot{M}$ , the larger the hard X-ray luminosity, and the softer the hard X-ray spectra. This behavior of the hard X-ray spectra of Cir X-1 is similar to that shown in Sco X-1, GX 17+2 (Di Salvo et al. 2000), and GX 349+2 (Di Salvo et al. 2001).

A possible origin of the power-law hard component is the Compton up scattering of soft X-ray seed photons by non-thermal electrons with a power-law velocity distribution (Iaria et al. 2001 b). These electrons could be part of a jet in a binary system. Similarly, a jet could also be the origin of the power-law hard component of the detected hard X-ray spectra of some Z sources such as GX 5-1, GX 17+2 (Di Salvo et al. 2000), and GX 349+2 (Di Salvo et al. 2001). So Cir X-1 shares the same origin of the power-law hard component with Z sources. It is another aspect that Cir X-1 shares with the Z source family.

The blackbody temperature is  $\sim 1$  keV, the blackbody component is probably emitted by the inner part of the accretion disk (Iaria et al. 2002). The bremsstrahlung seed-photon

temperature of the Comptonized component is 1.2-3.1 keV. A Gaussian emission line with energy  $\sim 6.5$  keV and an absorption edge with energy 8.2-9.2 keV are detected. The iron ionization of Fe<sub>XXIV–XXV</sub> corresponds to the emission line which is compatible with the absorption edge (Turner et al. 1992).

There shows an unusual line-like structure near 10 keV on the NB and FB (see Fig. 4 and Fig. 5). This result is consistent with that reported by Shirey et al.(1999). Asai et al. discuss several mechanisms that could possibly produce a line at  $\sim 10$  keV. For example, emission from a heavy element such as Ni could produce the line; a line could be blue-shifted due to motion in a relativistic jet or rotation in the accretion disk, but extreme conditions would be required to boost the energy up to  $\sim 10$  keV (Shirey et al. 1999). That there shows an unusual line near 10 keV in the FB spectrum (see Fig. 5) is the reason why the reduced  $\chi^2_\nu$  of this spectrum is as high as 2.54.

It is a key goal to distinguish neutron star (NS) binaries from black hole binaries (BHBs) in high energy astrophysics. Barret et al.(2000) suggested that only BHBs can have both X-ray (1-20 keV) and hard X-ray (20-200 keV) luminosities above  $1.5 \times 10^{37}$  ergs s<sup>-1</sup>. Using 5.5 kpc (Case et al. 1998) as the distance to Cir X-1, the luminosity of the power-law component in the 20-200 keV range is above  $1.5 \times 10^{37}$  ergs s<sup>-1</sup>. The reported total X-ray flux in the 2.5-25 keV band of Cir X-1 (Shirey et al. 1999) ranges over  $(4.39 - 2.72) \times 10^{-8}$  ergs cm<sup>-2</sup> s<sup>-1</sup>, thus the range of luminosity in the 2.5-25 keV range is  $L_{2.5-25}^{total} = (9.85 - 15.89) \times 10^{37}$  ergs s<sup>-1</sup>, and the X-ray (1-20 keV) luminosity must be above  $1.5 \times 10^{37}$  ergs s<sup>-1</sup>. As is well known, the compact object of Cir X-1 has been believed to be a neutron star because of the presence of type I X-ray bursts (Tennant et al, 1986 a, 1986 b), it seems that this luminosity criterion used to distinguish NS binaries from BHBs is not suitable to Cir X-1.

We appreciate the detailed comments and suggestions provided by the anonymous referee. This research has made use of data obtained through the High Energy Astrophysics Archive Research Center On-line Service, provided by NASA/Goddard Space Flight Center. We acknowledge the RXTE data teams at NASA/GSFC for their help. This work is subsidized by the Special Funds for Major State Basic Research Projects and by the National Science Foundation of China.

## REFERENCES

- Brandt, W. N., Fabian, A. C., Dotani, T., Nagase, F., Inoue, H., Kotani, T., & Segawa, Y. 1996, MNRAS, 283, 1071

- Barret, D., Olive, J. F., Boirin, L., Done, C., Skinner, G. K., & Grindlay, J. E. 2000, *ApJ*, 533, 329
- Case, G. L., & Bhattacharya, D. 1998, *ApJ*, 504, 761
- D’Amico, F., Heindl, W. A., Rothschild, R. E., & Gruber, D. E. 2001, *ApJ*, 547, 147
- Di Salvo, T., Stella, L., Robba, N. R., van der Klis, M., Burderi, L., Israel, G. L., Homan, J., Campana, S., Frontera, F., & Parmar, A. N. 2000, *ApJ*, 544, 119
- Di Salvo, T., Robba, N. R., Iaria, R., Stella, L., Burderi, L., & Israel, G. L. 2001, *ApJ*, 554, 49
- Glass, I. S. 1978, *MNRAS*, 183, 335
- Hasinger, G., & van der Klis, M. 1989, *A&A*, 225, 79
- Iaria, R., Di Salvo, T., Burderi, L., & Robba, N. R. 2001 a, *ApJ*, 561, 321
- Iaria, R., Burderi, L., Di Salvo, T., La Barbera, A., & Robba, N. R. 2001 b, *ApJ*, 547, 412
- Iaria, R., Di Salvo, T., Robba, N. R., & Burderi, L. 2002, *ApJ*, 567, 503
- Kaluzienski, L. J., Holt, S. S., Boldt, E. A., & Serlemitsos, P. J. 1976, *ApJ*, 208, 71
- van der Klis, M., Swank, J. H., Zhang, W., Jahoda, K., Morgan, E. H., Lewin, W. H. G., Vaughan, B., & van Paradijs, J. 1996, *ApJ*, 469, 1
- Moneti, A. 1992, *A&A*, 260, 7
- Oosterbroek, T., van der Klis, M., Kuulkers, E., van Paradijs, J., & Lewin, W. H. G. 1995, *A&A*, 297, 141
- Protassov, R. S., & Dyk, D. A. 2002, American Astronomical Society Meeting (AAS), 196, #54.01
- Qu, J. L., Yu, W., & Li, T. P. 2001, *ApJ*, 555, 7
- Rothschild, R. E., Blanco, P. R., Gruber, D. E., Heindl, W. A., MacDonald, D. R., Marsden, D. C., Pelling, M. R., Wayne, L. R., & Hink, P. L. 1998, *ApJ*, 496, 538
- Shirey, R. E. 1998, Ph.D. Thesis, MIT
- Shirey, R. E., Bradt, H. V., & Levine, A. M. 1999, *ApJ*, 517, 472

Toor, A. 1977, ApJ, 215, 57

Tennant, A. F., Fabian, A. C., & Shafer, R. A. 1986 a, MNRAS, 219, 871

Tennant, A. F., Fabian, A. C., & Shafer, R. A. 1986 b, MNRAS, 221, 27

Turner, T. J., Done, C., Mushotzky, R., & Madejski, G. 1992, ApJ, 391, 102

Whelan, J. A. J., Mayo, S. K., Wickramasinghe, D. T., Murdin, P. G., Peterson, B. A.,  
Hawarden, T. G., Longmore, A. J., Haynes, R. F., Goss, W. M., Simons, L. W.,  
Caswell, J. L., Little, A. G., & McAdam, W. B. 1977, MNRAS, 181, 259

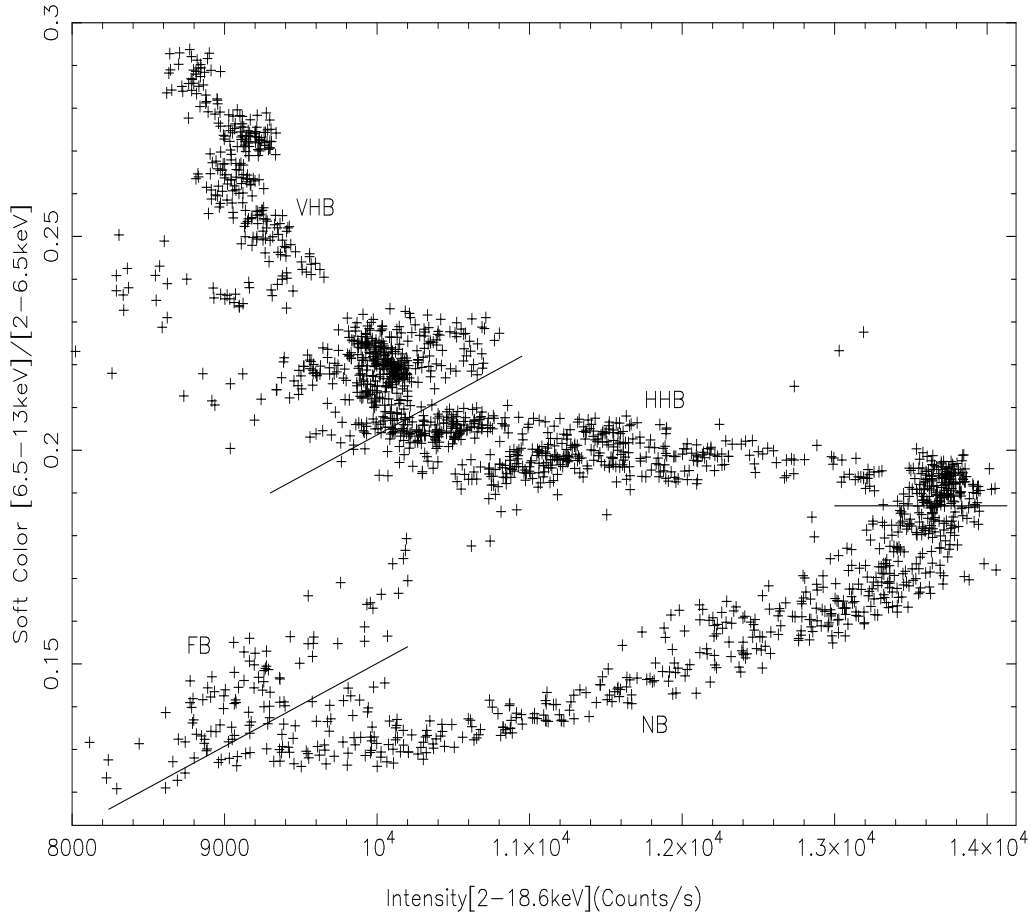


Fig. 1.— The HID of Cir X-1. Each point is from 16 s background-subtracted data from PCU012.

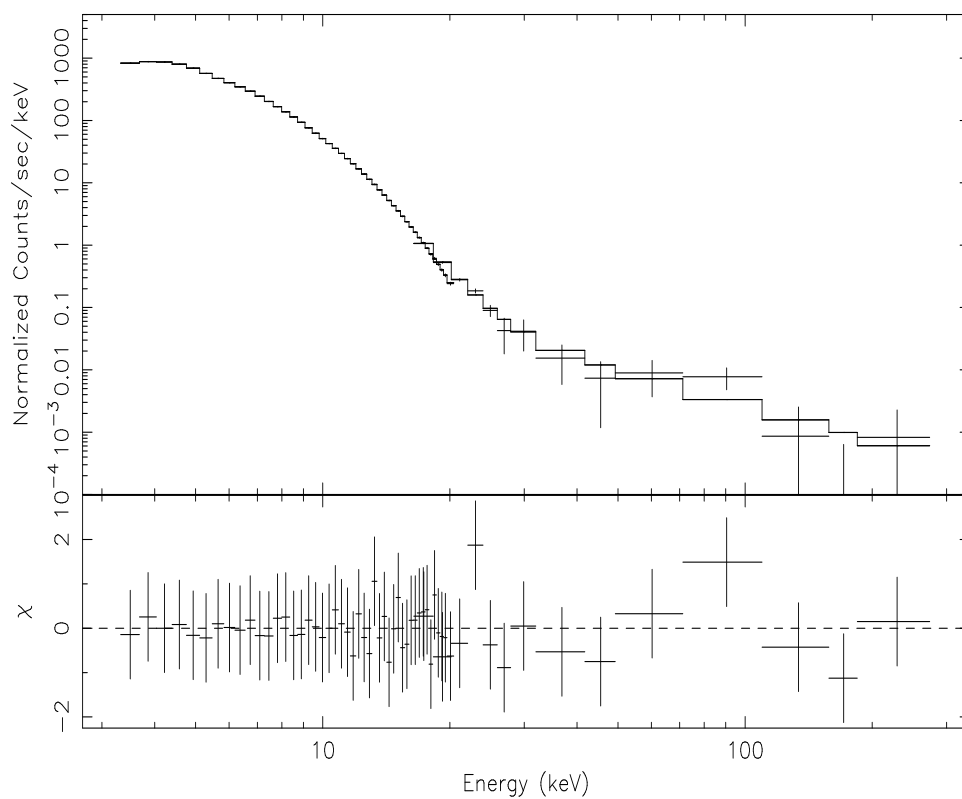


Fig. 2.— The VHB Spectrum of Cir X-1. The spectrum results from 17570 s PCA (PCU0 only) and 12290 s good HEXTE data. A combination model of Bbody+Line+Bremss+Power-law+Edge fits to the observed spectrum with 1% systematic error being set to the PCA data. The reduced  $\chi^2_\nu$  is 0.37.

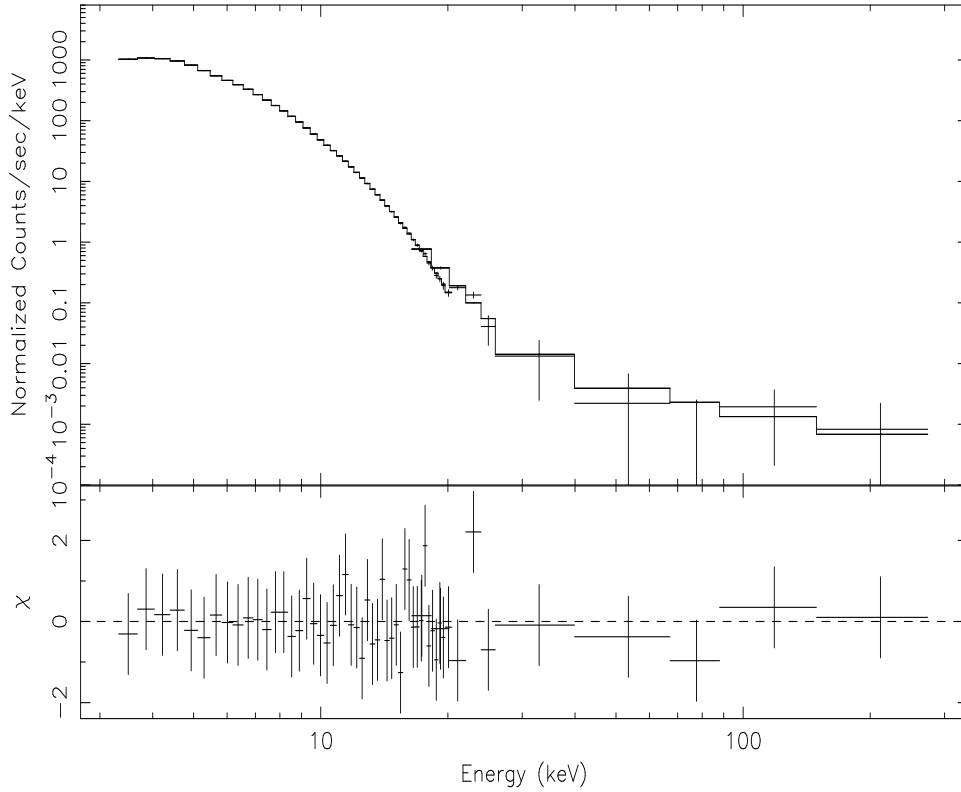


Fig. 3.— The HHB Spectrum of Cir X-1. The spectrum results from 8130 s PCA (PCU0 only) data and 12723 s good HEXTE data. A combination model of Bbody+Line+Bremss+Power-law+Edge fits to the observed spectrum with 1% systematic error being set to the PCA data and the Line of  $E=6.50$  keV being frozen. The reduced  $\chi^2_\nu$  is 0.57.

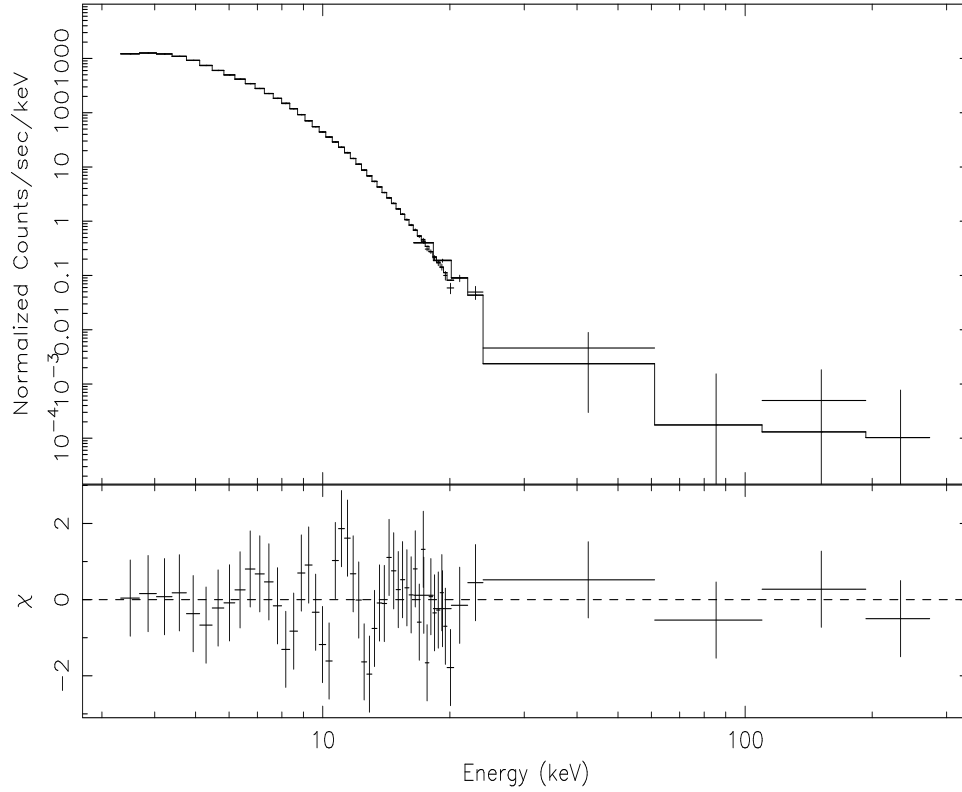


Fig. 4.— The NB Spectrum of Cir X-1. The spectrum results from 10160 s PCA (PCU0 only) data and 14980.0 s good HEXTE data and is fit by a combination model of Bbody+Line+Bremss+Power-law+Edge with 1% systematic error being set to the PCA data and the Line of  $E=6.50$  keV being frozen. The reduced  $\chi^2_{\nu}$  is 0.94. There shows an unusual line near 10 keV in this spectrum.

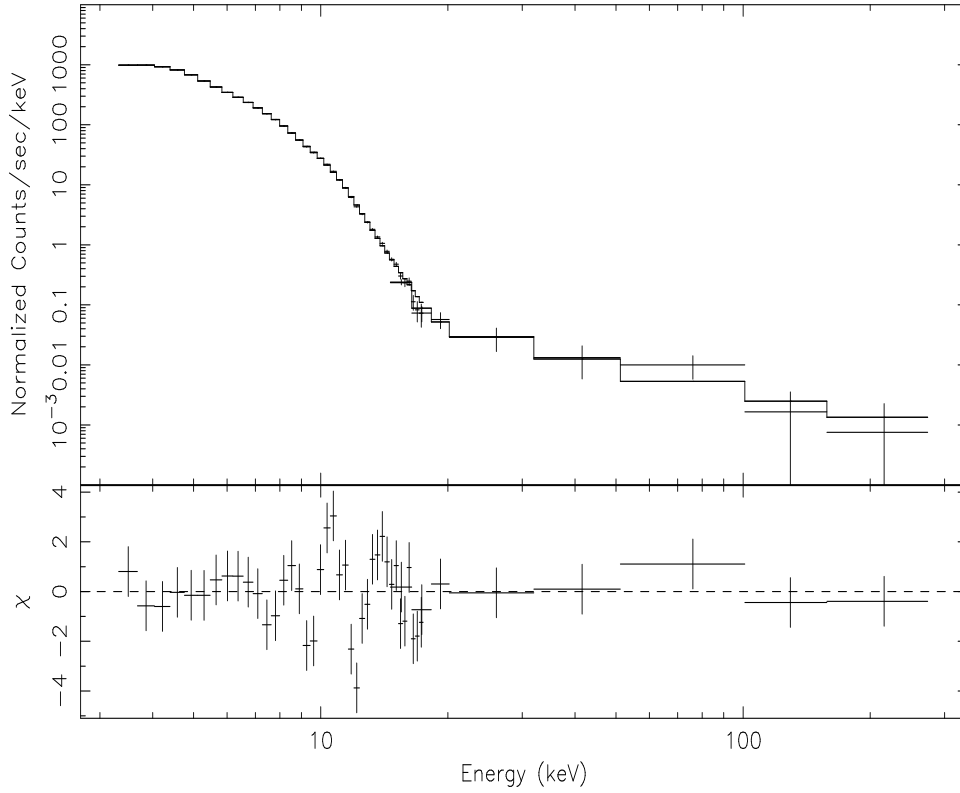


Fig. 5.— The FB Spectrum of Cir X-1. The spectrum results from 6920 s PCA (PCU0 only) data and 5130.0 s good HEXTE data and is fit by a combination model of Bbody+Line+Bremss+Power-law+Edge with 1% systematic error being set to the PCA data and the Line at 6.50 keV being frozen. The reduced  $\chi^2_\nu$  is 2.54. That there shows an unusual line near 10 keV in this spectrum is the reason why the reduced  $\chi^2_\nu$  of this spectrum is high.

Table 1: The used RXTE observations of Cir x-1

OBSID	MJD	HID Pos.	PCA observation	HEXTE observation
			Time Interval (s)	Good Time Interval (s)
20094-01-02-020	49353	VHB	17570.0	12290.0
20094-01-02-020	49353	HHB	8130.0	6265.0
20094-01-02-020	49353	NB	2352.0	2299.0
20094-01-02-02	49353	NB	7808.0	6426.0
20094-01-02-02	49353	FB	6920.0	4290.0
20094-01-02-100	49353	HHB	12500.0	6458.0
20094-01-02-100	49353	NB	4672.0	2665.0
20094-01-02-09	49353	FB	1100.0	840.0
20094-01-02-09	49353	NB	11250.0	3590.0

Table 2: The Fit Parameters

HID Pos.	VHB	HHB	NB	FB
$N_H$ ( $\times 10^{22}$ cm $^{-2}$ )	$3.02^{+0.66}_{-0.60}$	$2.61^{+1.56}_{-0.75}$	$12.88^{+1.85}_{-2.86}$	$13.25^{+2.46}_{-2.68}$
$kT_{bb}$ (keV)	$1.021^{+0.052}_{-0.059}$	$1.026^{+0.023}_{-0.032}$	$0.95^{+0.11}_{-0.14}$	$0.785^{+0.049}_{-0.045}$
$E_{line}$ (keV)	$6.48^{+0.23}_{-0.43}$	6.50 (frozen)	6.50 (frozen)	6.50 (frozen)
$E_{edge}$ (keV)	$9.12^{+0.34}_{-0.25}$	$9.19^{+0.21}_{-0.19}$	$8.820^{+0.085}_{-0.044}$	$8.284^{+0.068}_{-0.068}$
$kT_{bremss}$ (keV)	$2.92^{+0.39}_{-0.50}$	$3.04^{+0.46}_{-0.64}$	$2.89^{+0.47}_{-0.44}$	$1.215^{+0.030}_{-0.022}$
$\Gamma_{power-law}$ (PhoIndex)	$2.11^{+2.22}_{-0.69}$	$1.58^{+8.42}_{-1.32}$	0.95 (frozen)	$1.62^{+0.69}_{-0.41}$
$\chi^2$ ( <i>dof</i> )	16.08 (44)	23.36 (41)	37.47 (40)	81.21 (32)

Note. — Blackbody+Line+Bremsstrahlung+Power-law+Edge model is used. Uncertainties are given at 90% confidence level for the derived parameters of the model applied.

Table 3: The Estimated Absorbed Fluxes and Luminosity

HID Pos.	Flux	Flux	Flux	Luminosity
	Bremsstrahlung 3-200 keV	Power-law 20-200 keV	All Components 3-200 keV	All Components 3-200 keV
VHB	5.43	10.14	16.10	5.83
HHB	4.97	4.81	10.69	3.87
NB	2.81	0.40	5.36	1.94
FB	0.34	10.30	13.02	4.71

Note. — The fluxes are in units of  $10^{-8}$  ergs  $\text{cm}^{-2}$   $\text{s}^{-1}$ . The luminosity is in units of  $10^{38}$  ergs  $\text{s}^{-1}$ , assuming a distance of the source of 5.5 kpc (Case et al. 1988).

Table 4: F-test of The Four Spectra

HID Pos.	Bbody+Line+Bremss +Edge	Bbody+Line+Bremss +Power-law+Edge	F-test Probability
	$\chi^2$ ( <i>dof</i> )	$\chi^2$ ( <i>dof</i> )	
VHB	31.48 (48)	16.08 (44)	$4.49 \times 10^{-6}$
HHB	31.64 (45)	23.36 (41)	$1.27 \times 10^{-2}$
NB	60.99 (43)	37.47 (40)	$1.94 \times 10^{-4}$
FB	142.08 (36)	81.21 (32)	$1.02 \times 10^{-3}$